Journal of Marine Science and Engineering

Article

Underwater Sound Speed Field Forecasting Based on the Least Square Support Vector Machine

Junting Wang [1], Tianhe Xu [1,*], Wei Huang [2], Liping Zhang [3], Jianxu Shu [1], Yangfan Liu [1] and Linyang Li [4]

1 Shandong Key Laboratory of Optical Astronomy and Solar-Terrestrial Environment, Institute of Space Science, Shandong University, Weihai 264209, China; wangjunting@sdu.edu.cn (J.W.); shujx@mail.sdu.edu.cn (J.S.); liuyangfan1995@163.com (Y.L.)
2 Faculty of Information Science and Engineering, Ocean University of China, Qingdao 266100, China; hw@ouc.edu.cn
3 State Key Laboratory of Geo-Information Engineering, Xi'an 710054, China; zlp_791225@126.com
4 College of Geology Engineering and Geomantic, Chang'an University, Xi'an 710064, China; chdxxb@163.com
* Correspondence: thxu@sdu.edu.cn

Abstract: Underwater sound speed is one of the most significant factors that affects high-accuracy underwater acoustic positioning and navigation. Due to its complex temporal variation, the forecasting of the underwater sound speed field (SSF) becomes a challenging task. Taking advantage of machine learning methods, we propose a new method for SSF forecasting based on the least square support vector machine (LSSVM) and a multi-parameter model, aiming to enhance the forecasting accuracy of underwater SSF with hourly resolution. We first use a matching extension method to standardize profile data and train the LSSVM with the parameters of observation time, temperature, salinity, and depth. We then employ radial basis function kernels to construct the forecasting model of SSF. We validate the feasibility and effectiveness of the LSSVM model by comparing it with the polynomial fitting (PF) and back propagation neural network (BPNN) methods, using hourly data obtained from the measured data and open data. The results show that the means of the root mean square for the LSSVM based on the observation time parameter and the LSSVM based on the multi-parameter model achieve 0.51 m/s and 0.45 m/s, respectively, presenting a significant improvement compared with the PF (0.82 m/s) and BPNN (0.76 m/s) methods.

Keywords: forecasting model; sound speed field (SSF); least square support vector machine (LSSVM); matching extension; empirical orthogonal function (EOF)

Citation: Wang, J.; Xu, T.; Huang, W.; Zhang, L.; Shu, J.; Liu, Y.; Li, L. Underwater Sound Speed Field Forecasting Based on the Least Square Support Vector Machine. *J. Mar. Sci. Eng.* **2024**, *12*, 480. https://doi.org/10.3390/jmse12030480

Academic Editor: Eugen Rusu

Received: 26 January 2024
Revised: 2 March 2024
Accepted: 12 March 2024
Published: 13 March 2024

1. Introduction

In the marine environment, acoustic signals serve as the primary signal carriers of underwater positioning, navigation, timing, and communication (PNTC) systems [1–3]. However, the propagation speed of underwater acoustic signals has complex characteristics in terms of spatial–temporal dynamics [4], which leads to the bending effect of the signal propagation path. This issue presents challenges to the efficient utilization of beam energy in directional underwater acoustic communication systems, as well as precise ranging for underwater acoustic positioning and navigation [5,6]. Therefore, to obtain high precision and high resolution, regional sound speed fields (SSFs) have become a key technology in underwater PNTC systems. The main methods for obtaining underwater sound speed profiles (SSPs) include the direct measurement and the inversion of SSPs. The sound speed profiler (SSP), the conductivity temperature depth (CTD), and the expendable conductivity–temperature–depth (XCTD) profiler are used to measure SSPs [7]. Due to the limited observation depth of XCTD, the measured SSP, temperature profile (TP), and salinity profiles (SP) cannot cover the full ocean depth. Furthermore, since the marine environment often changes with time and space, it is time-consuming and labor-intensive to measure the sound speed from point to point.

In order to eliminate the representative measurement error of sound speed, the inversion method of sound speed based on measured historical SSPs was developed to construct SSFs with high resolution. Munk and Wunsch [8] introduced geophysical inversion methods into marine physics and creatively proposed the concept of ocean acoustic tomography. As one of the branches of ocean acoustic tomography, sound speed inversion uses ocean environmental parameters to construct the distribution of SSFs in a target spatiotemporal region. The inversion technology of sound speed mainly focuses on the interpolation or extrapolation of sound speed based on position and time information, matched field processing, compressive sensing, and deep learning. The matched field processing method uses empirical orthogonal function (EOF) or singular value decomposition (SVD) to perform principal component analysis for the SSP [9], and selects the matched beam, the matched propagation time, or the matched multipath time difference to achieve the inversion of the SSF [10–12]. Davis [13] proved that the EOF is the most effective basis function for describing the sound speed profile in the sense of the minimum mean square error. Bianco et al. [14] proposed that SVD should be used instead of EOF decomposition to reduce the number of eigenvectors. Tolstoy et al. [15] proposed a matching field processing method based on EOF for principal component analysis, which used the lattice traversal method to search for matching terms to invert the SSP. In order to accelerate the search process, the inversion of the SSF—based on particle swarm optimization (PSO), simulated annealing (SA), and genetic algorithm (GA)—was developed to improve the efficiency of searching the principal component coefficient for SSP feature vectors [16,17]. Although the computational efficiency can be improved by a matched field algorithm combining heuristic algorithms, it should be noted that the computational complexity of the algorithm is relatively high, and its inversion accuracy is affected by the beam propagation delay. The principal component coefficients and the least squares algorithm are used to construct the SSF in the compressive sensing method. Bianco et al. and Choo et al. [18,19] proposed the inversion method of sound speed based on compressive sensing and EOF decomposition. Compared with matched field processing, the inversion efficiency of compressive sensing is significantly improved, but the compressive sensing dictionary establishment process adopts first-order Taylor expansion for linear approximation, which reduces the inversion accuracy.

Since the marine environment is complex and changeable, it is hard to accurately construct the sound speed model with a linear system or deterministic mathematical expression [20]. Machine learning algorithms offer a distinct advantage of fitting complex nonlinear functions, which are suitable for solving the inversion problem of SSFs. The application of deep learning techniques to sound speed inversion can be broadly categorized into two approaches: those that utilize acoustic time delay observation data and those that do not. For deep learning with acoustic time delay observation data, Stephan et al. [21] firstly established the inversion framework of SSF by using an artificial neural network (ANN). Ai et al. [22] constructed the SSF by using the back propagation neural network (BPNN) combined with the EOF. The inversion accuracy of SSF based on the neural network is affected by the acoustic time delay observation and the EOF order selection, and the method requires a large number of historical SSPs as reference samples. Aiming for the SSF construction of small sample, a task-driven meta learning (TDML) framework for constructing SSFs was proposed to achieve model convergence [23]. For deep learning without acoustic time delay observation data, Zhang et al. [24] proposed the four-layer piecewise function with nine parameters to describe the sound speed structure of the mixed layer, the main thermocline, and the deep-sea isothermal layer, respectively. Zhang et al. [16] utilized the nonlinear input–output characteristics of neural networks to train complex seawater salinity parameters, and established the BPNN model. Luo et al. [25] constructed the mapping relationship between the sound speed and the sediment physical parameter using the BPNN method. The above methods construct a large-scale SSF based on multiple parameters, and its accuracy is based on a large number of referenced SSPs.

For underwater acoustic positioning and navigation, the temporal variation of sound speed has a greater impact on positioning and navigation accuracy compared with the spatial variation of sound speed [26]. Constructing the SSF with hourly resolution can effectively eliminate the representativeness error of sound speed. To predict the SSF constructed with hourly resolution, three major challenges need to be addressed: (1) how to extend the profile data to construct the SSF of the full ocean depth; (2) how to construct the inversion method of SSFs based on small samples; (3) how to construct the inversion model of SSFs made with hourly resolution. Therefore, this paper proposes an SSF forecasting method based on the least square support vector machine (LSSVM) considering multiple parameters. The proposed algorithm is validated by measured and public data. By comparing sound speed data obtained from equipment, polynomial fitting, BPNN, LSSVM with an observation time parameter, and LSSVM with multiple parameters, we assessed the accuracy of different algorithms against actual values.

The paper is organized as follows. We begin by presenting the matching extension method based on EOF in Section 2. Section 3 introduces the forecasting method of SSF based on polynomial fitting and BPNN, as well as the theoretical derivation and algorithm implementation of the SSF forecasting method based on the LSSVM. The polynomial fitting method, the BPNN method, the LSSVM based on the observation time parameter, and the LSSVM based on multiple parameters are verified and analyzed using both the measured data and public data in Section 4. Finally, we summarize the significant conclusions in Section 5.

2. Matching Extension Method Based on EOF

Because the SSP, TP, and SP collected by XCTD cannot cover the full depth, the XCTD data must be extended to provide the measured dataset of full ocean depth in order to construct the forecasting model of SSF. We propose a matching extension method based on EOF, and the basic steps of the matching extension method are as follows:

(1) Let measured SSPs, TPs, and SPs with full ocean depth set $\boldsymbol{S} = \{\boldsymbol{S}_1, \boldsymbol{S}_2, \ldots, \boldsymbol{S}_i\}$, $\boldsymbol{T} = \{\boldsymbol{T}_1, \boldsymbol{T}_2, \ldots, \boldsymbol{T}_i\}$, and $\boldsymbol{A} = \{\boldsymbol{A}_1, \boldsymbol{A}_2, \ldots, \boldsymbol{A}_i\}$. Each SSP, TP, and SP sample could be expressed as

$$\begin{cases} \boldsymbol{S}_i = \left\{(s_{i,1}, d_1), (s_{i,2}, d_2), \ldots, \left(s_{i,j}, d_j\right)\right\} \\ \boldsymbol{T}_i = \left\{(t_{i,1}, d_1), (t_{i,2}, d_2), \ldots, \left(t_{i,j}, d_j\right)\right\} \\ \boldsymbol{A}_i = \left\{(a_{i,1}, d_1), (a_{i,2}, d_2), \ldots, \left(a_{i,j}, d_j\right)\right\} \end{cases} \tag{1}$$

where $s_{i,j}$, $t_{i,j}$, and $a_{i,j}$ are sound speed, temperature, and salinity, respectively, and d_j is the depth. $i = 1, 2, \ldots, I$ means the i-th sample; $j = 1, 2, \ldots, J$ is the index label of depth; and d_J is the maximum sampling depth with full depth. If the maximum depth of the target SSP (TP, SP) to be extended is d_K, all SSPs, TPs, and SPs in $\boldsymbol{S}$, $\boldsymbol{T}$, and $\boldsymbol{A}$ are partially intercepted by depth and form a dataset of reference SSPs—$\overline{\boldsymbol{S}} = \left\{\overline{\boldsymbol{S}_1}, \overline{\boldsymbol{S}_2}, \ldots, \overline{\boldsymbol{S}_i}\right\}$, TPs $\overline{\boldsymbol{T}} = \left\{\overline{\boldsymbol{T}_1}, \overline{\boldsymbol{T}_2}, \ldots, \overline{\boldsymbol{T}_i}\right\}$, and SPs $\overline{\boldsymbol{A}} = \left\{\overline{\boldsymbol{A}_1}, \overline{\boldsymbol{A}_2}, \ldots, \overline{\boldsymbol{A}_i}\right\}$, $i = 1, 2, \ldots, I$ with a maximum depth that equals d_K, where $\overline{\boldsymbol{S}}_i$, $\overline{\boldsymbol{T}}_i$, and $\overline{\boldsymbol{A}}_i$ can be expressed as

$$\begin{cases} \overline{\boldsymbol{S}}_i = \left\{(s_{i,1}, d_1), (s_{i,2}, d_2), \ldots, (s_{i,k}, d_k)\right\} \\ \overline{\boldsymbol{T}}_i = \left\{(t_{i,1}, d_1), (t_{i,2}, d_2), \ldots, (t_{i,k}, d_k)\right\} \\ \overline{\boldsymbol{A}}_i = \left\{(a_{i,1}, d_1), (a_{i,2}, d_2), \ldots, (a_{i,k}, d_k)\right\} \end{cases} \tag{2}$$

where $k = 1, 2, \ldots, K$.

(2) To maintain the original principal component of any target SSP (TP, SP) to be extended, the feature vectors of reference SSPs (TPs, SPs) and the target SSP are obtained through EOF. These are calculated by

$$\begin{cases} \boldsymbol{SV}_{d_J} = \left[sv_{1,d_J}, sv_{2,d_J}, \ldots, sv_{m,d_J}\right], m = 1, 2, \ldots, \overline{M} \\ \boldsymbol{SV}_{d_K} = \left[sv_{1,d_K}, sv_{2,d_K}, \ldots, sv_{n,d_K}\right], n = 1, 2, \ldots, \overline{N} \end{cases} \tag{3}$$

$$\begin{cases} \boldsymbol{TV}_{d_J} = \left[tv_{1,d_J}, tv_{2,d_J}, \ldots, tv_{m,d_J}\right], m = 1,2,\ldots,\overline{M} \\ \boldsymbol{TV}_{d_K} = \left[tv_{1,d_K}, tv_{2,d_K}, \ldots, tv_{n,d_K}\right], n = 1,2,\ldots,\overline{N} \end{cases} \tag{4}$$

$$\begin{cases} \boldsymbol{AV}_{d_J} = \left[av_{1,d_J}, av_{2,d_J}, \ldots, av_{m,d_J}\right], m = 1,2,\ldots,\overline{M} \\ \boldsymbol{AV}_{d_K} = \left[av_{1,d_K}, av_{2,d_K}, \ldots, av_{n,d_K}\right], n = 1,2,\ldots,\overline{N} \end{cases} \tag{5}$$

where $\boldsymbol{SV}_{d_J}$, $\boldsymbol{TV}_{d_J}$, and $\boldsymbol{AV}_{d_J}$ are the feature vectors of reference SSPs, TPs, and SPs, respectively. $\boldsymbol{SV}_{d_K}$, $\boldsymbol{TV}_{d_K}$, and $\boldsymbol{AV}_{d_K}$ are the feature vectors of target SSPs, TPs, and SPs, respectively. m and n are the order of the feature vector, and $\overline{M}$ and $\overline{N}$ are the total number of orders, which satisfies $3 \le \overline{M}, \overline{N} \le 5$.

(3) Through the matching process, the coefficients $\boldsymbol{sf}_{d_K}$, $\boldsymbol{tf}_{d_K}$, and $\boldsymbol{af}_{d_K}$ could be solved by

$$\begin{cases} \boldsymbol{sf}_{d_K} = \boldsymbol{SV}_{d_K}^{\boldsymbol{T}}\left(\boldsymbol{S}_t^g - \overline{\boldsymbol{S}}_{ar,d_K}\right) \\ \boldsymbol{S}_t^g = \left[s_{t,1}, s_{t,2}, \ldots, s_{t,k}\right] \\ \overline{\boldsymbol{S}}_{ar,d_K} = \left[\overline{s}_{ar,d_1}, \overline{s}_{ar,d_2}, \ldots, \overline{s}_{ar,d_k}\right] \end{cases} \tag{6}$$

$$\begin{cases} \boldsymbol{tf}_{d_K} = \boldsymbol{TV}_{d_K}^{\boldsymbol{T}}\left(\boldsymbol{T}_t^g - \overline{\boldsymbol{T}}_{ar,d_K}\right) \\ \boldsymbol{T}_t^g = \left[t_{t,1}, t_{t,2}, \ldots, t_{t,k}\right] \\ \overline{\boldsymbol{T}}_{ar,d_K} = \left[\overline{t}_{ar,d_1}, \overline{t}_{ar,d_2}, \ldots, \overline{t}_{ar,d_k}\right] \end{cases} \tag{7}$$

$$\begin{cases} \boldsymbol{af}_{d_K} = \boldsymbol{AV}_{d_K}^{\boldsymbol{T}}\left(\boldsymbol{A}_t^g - \overline{\boldsymbol{A}}_{ar,d_K}\right) \\ \boldsymbol{A}_t^g = \left[a_{t,1}, a_{t,2}, \ldots, a_{t,k}\right] \\ \overline{\boldsymbol{A}}_{ar,d_K} = \left[\overline{a}_{ar,d_1}, \overline{a}_{ar,d_2}, \ldots, \overline{a}_{ar,d_k}\right] \end{cases} \tag{8}$$

where $\boldsymbol{S}_t^g$, $\boldsymbol{T}_t^g$, and $\boldsymbol{A}_t^g$ are the target SSP, TP, and SP, respectively. $\overline{\boldsymbol{S}}_{ar,d_K}$, $\overline{\boldsymbol{T}}_{ar,d_K}$, and $\overline{\boldsymbol{A}}_{ar,d_K}$ are the average SSP, TP, and SP distribution of $\overline{\boldsymbol{S}}$, $\overline{\boldsymbol{T}}$, and $\overline{\boldsymbol{A}}$, respectively.

(4) When combining $\boldsymbol{sf}_{d_K}$, $\boldsymbol{tf}_{d_K}$, and $\boldsymbol{af}_{d_K}$ with $\boldsymbol{SV}_{d_J}$, $\boldsymbol{TV}_{d_J}$, and $\boldsymbol{AV}_{d_J}$, the target SSP, TP, and SP with full ocean depth will be constructed:

$$\begin{cases} \hat{\boldsymbol{S}}_t^g = \boldsymbol{S}_{ar,d_J}^g + \boldsymbol{SV}_{d_J}\boldsymbol{sf}_{d_K} \\ \hat{\boldsymbol{T}}_t^g = \boldsymbol{T}_{ar,d_J}^g + \boldsymbol{TV}_{d_J}\boldsymbol{tf}_{d_K} \\ \hat{\boldsymbol{A}}_t^g = \boldsymbol{A}_{ar,d_J}^g + \boldsymbol{AV}_{d_J}\boldsymbol{af}_{d_K} \end{cases} \tag{9}$$

where $\boldsymbol{S}_{ar,d_J}^g = \left[s_{ar,d1}, s_{ar,d2}, \ldots, s_{ar,dJ}\right]$, $\boldsymbol{T}_{ar,d_J}^g = \left[t_{ar,d1}, t_{ar,d2}, \ldots, t_{ar,dJ}\right]$, $\boldsymbol{A}_{ar,d_J}^g = \left[a_{ar,d1}, a_{ar,d2}, \ldots, a_{ar,dJ}\right]$, and $\hat{\boldsymbol{S}}_t^g = \left[\hat{s}_{t,1}, \hat{s}_{t,2}, \ldots, \hat{s}_{t,J}\right]$, $\hat{\boldsymbol{T}}_t^g = \left[\hat{t}_{t,1}, \hat{t}_{t,2}, \ldots, \hat{t}_{t,J}\right]$, $\hat{\boldsymbol{A}}_t^g = \left[\hat{a}_{t,1}, \hat{a}_{t,2}, \ldots, \hat{a}_{t,J}\right]$.

3. Methodology for Constructing the Forecasting Model of Sound Speed Fields

3.1. Forecasting of SSFs Based on Polynomial Fitting

The forecasting method of SSFs based on polynomial fitting maps the nonlinear relationship between the sound speed and the observation time at depth d_k using historical SSP data. The functional model of observation time and the vertical gradient of sound speed can be obtained through polynomial fitting. The basic steps of the polynomial fitting algorithm are given as follows:

(1) After the matching extension of SSP, the dataset of reference SSPs for SSF forecasting can be obtained as

$$S_r = \{(s_{r,1}, d_1), (s_{r,2}, d_2), \cdots, (s_{r,k}, d_k)\}, r = 1,2,\cdots R, k = 1,2,\cdots K \tag{10}$$

where R is the number of reference SSPs.

(2) The nonlinear relationship between the sound speed and the observation time at depth d_k is constructed as

$$S_{r,k} = \alpha_k + \beta_k \tau_r + \phi_k * sin(2\tau_r \pi / 86400 + \omega_k) \quad (11)$$

where $X_k = [\alpha_k, \beta_k, \phi_k, \omega_k]$ is the model parameter vector, τ_r is the observation time of measuring SSPs.

(3) R-th SSPs are used to construct the SSF; the linearization matrix form of Equation (11) can be expressed as:

$$\begin{bmatrix} s_{1,k} \\ s_{2,k} \\ \vdots \\ s_{r,k} \end{bmatrix} - \begin{bmatrix} s^0_{1,k} \\ s^0_{2,k} \\ \vdots \\ s^0_{r,k} \end{bmatrix} = \begin{bmatrix} 1 & \tau_1 & sin(2\tau_1\pi/86400 + \omega^0_k) & cos(2\tau_1\pi/86400 + \omega^0_k) \\ 1 & \tau_2 & sin(2\tau_2\pi/86400 + \omega^0_k) & cos(2\tau_2\pi/86400 + \omega^0_k) \\ \vdots & \vdots & \vdots & \vdots \\ 1 & \tau_r & sin(2\tau_r\pi/86400 + \omega^0_k) & cos(2\tau_r\pi/86400 + \omega^0_k) \end{bmatrix} \begin{bmatrix} \Delta\alpha_k \\ \Delta\beta_k \\ \Delta\phi_k \\ \Delta\omega_k \end{bmatrix} \quad (12)$$

$$s^0_{r,k} = \alpha^0_k + \beta^0_k \tau_r + \phi^0_k * sin\left(2\tau_r \pi / 86400 + \omega^0_k\right) \quad (13)$$

where $\boldsymbol{X}^0_k = [\alpha^0_k, \beta^0_k, \phi^0_k, \omega^0_k]$ is the approximate value of the model parameter, $\boldsymbol{x}_k = [\Delta\alpha_k, \Delta\beta_k, \Delta\phi_k, \Delta\omega_k]$ is the correction vector of the model parameter. Based on Equation (12), the error equation is constructed by

$$\boldsymbol{L}_{r,k} + \boldsymbol{V}_{r,k} = \boldsymbol{A}_{r,k}\boldsymbol{x}_k \quad (14)$$

According to the least squares,

$$\boldsymbol{x}_k = \left(\boldsymbol{A}^T_{r,k}\boldsymbol{A}_{r,k}\right)^{-1}\boldsymbol{A}^T_{r,k}\boldsymbol{L}_{r,k} \quad (15)$$

$$\boldsymbol{X}_k = \boldsymbol{X}^0_k + \boldsymbol{x}_k \quad (16)$$

where $\boldsymbol{L}_{r,k}$ is the observation vector of Equation (14), $\boldsymbol{V}_{r,k}$ is the residual vector of $\boldsymbol{L}_{r,k}$, and $\boldsymbol{A}_{r,k}$ is the design matrix of Equation (14).

(4) When the observation time of the forecasting SSP is τ_f, the SSP at depth d_k is calculated by

$$s_{f,k} = \alpha_k + \beta_k \tau_f + \phi_k * sin(2\tau_r \pi / 86400 + \omega_k) \quad (17)$$

(5) Repeating step (1) to step (4), the forecasting SSP $\boldsymbol{S}_f = \left\{\left(s_{f,0}, d_0\right), \left(s_{f,1}, d_1\right), \cdots, \left(s_{f,k}, d_k\right)\right\}$ of full depth can be obtained.

3.2. Forecasting of SSFs Based on BPNN

The BPNN algorithm has advantages in nonlinear function fitting and its algorithm efficiency is high after the training model converges. Therefore, BPNN is used to construct the sound speed field [20]. The forecasting method of SSF based on the BPNN algorithm regards the unknown system as a black box—it can express the nonlinear relationships between the sound speed and the observation time, the temperature, and the salinity at depth d_k using historical SSP data. However, the method has disadvantages in small sample learning. The network structure of BPNN is shown in Figure 1 [20,27].

For the BPNN method, the input layer of the training set is expressed as

$$\begin{cases} \boldsymbol{\tau}_{\text{in}} = [(\tau_1, \cdots, \tau_r \cdots, \tau_R)_1, \cdots, (\tau_1, \cdots, \tau_r \cdots, \tau_R)_k, \cdots, (\tau_1, \cdots, \tau_r \cdots, \tau_R)_K] \\ \boldsymbol{d}_{\text{in}} = [(d_1, \cdots, d_r \cdots, d_R)_1, \cdots, (d_1, \cdots, d_r \cdots, d_R)_k, \cdots, (d_1, \cdots, d_r \cdots, d_R)_K] \\ \boldsymbol{t}_{\text{in}} = [(t_1, \cdots, t_r \cdots, t)_1, \cdots, (t_1, \cdots, t_r \cdots, t_R)_k, \cdots, (t_1, \cdots, t_r \cdots, t_R)_K] \\ \boldsymbol{a}_{\text{in}} = [(a_1, \cdots, a_r \cdots, a_R)_1, \cdots, (a_1, \cdots, a_r \cdots, a_R)_k, \cdots, (a_1, \cdots, a_r \cdots, a_R)_K] \end{cases} \quad (18)$$

where $\boldsymbol{\tau}_{\text{in}}$, $\boldsymbol{d}_{\text{in}}$, $\boldsymbol{t}_{\text{in}}$, and $\boldsymbol{a}_{\text{in}}$ are the input vectors of the observation time, depth, temperature, and salinity in the training set, respectively.

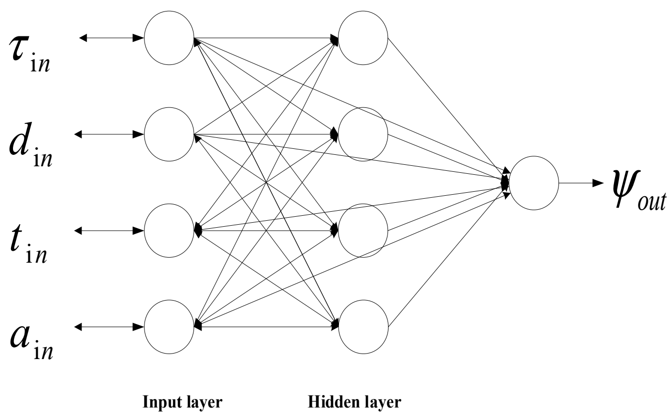

Figure 1. Flowchart for SSF forecasting using BPNN.

The output layer of the training set is given as

$$\boldsymbol{s}_{out} = [(s_1, \cdots, s_r \cdots, s_R)_1, \cdots, (s_1, \cdots, s_r \cdots, s_R)_k, \cdots, (s_1, \cdots, s_r \cdots, s_R)_K] \tag{19}$$

where $\boldsymbol{s}_{out}$ is the output vector of the sound speed in the training set.

The input layer of the forecasting set is

$$\boldsymbol{\vartheta}_{\text{in}} = \left[\left(\tau_{f,1}, d_{f,1}, t_{f,1}, a_{f,1}\right), \cdots, \left(\tau_{f,k}, d_{f,k}, t_{f,k}, a_{f,k}\right), \cdots, \left(\tau_{f,K}, d_{f,K}, t_{f,K}, a_{f,K}\right)\right] \tag{20}$$

where $\boldsymbol{\vartheta}_{\text{in}}$ represents the input vectors of the observation time, depth, temperature, and salinity in the forecasting set.

The output layer of the forecasting set is

$$\boldsymbol{\Psi}_{out} = \left[s_{f,1}, \cdots, s_{f,k}, \cdots, s_{f,K}\right] \tag{21}$$

where $\boldsymbol{\Psi}_{out}$ is the output vector of the sound speed in the forecasting set.

Because the network structure of BPNN has only one output node, the number of hidden layers in BPNN is a single hidden layer. The equation for the optimal number of hidden layer nodes can be expressed as [20]

$$hidden < \sqrt{|\kappa_{in} - \kappa_{out}|} + \eta \tag{22}$$

where κ_{in} and κ_{out} are the number of input and output layer nodes. η is a constant between 1 and 10.

The selection of hidden layer nodes first refers to Equation (22) to determine the approximate range of the number of nodes, and then the recurrent optimization method is used to determine the optimal number of nodes [28]. The number of hidden layer nodes in the BPNN structure of Figure 1 is four. The node transfer function is expressed as a tansig function in BPNN. At the same time, choosing the right parameter configuration can improve calculation efficiency and accuracy. The number of iterations is chosen as 300; the learning rate is 0.5; and the target is 0.0004 for sound speed field forecasting based on BPNN in this paper.

3.3. Forecasting of SSFs Based on the LSSVM

The forecasting method of SSFs based on the LSSVM transforms the problem of model construction into the problem of linear least squares in high dimensional space [29]. The method constructs a function that reflects the temporal variation characteristics of sound speed through the selection of kernel functions and training samples. The least-squares version of the support vector machine (SVM) classifier is obtained by reformulating the minimization problem as [30]

$$min\xi(\boldsymbol{\psi}, e_r) = \frac{1}{2}\boldsymbol{\psi}^T\boldsymbol{\psi} + \frac{1}{2}\gamma\sum_{r=1}^{R} e_r^2 \tag{23}$$

subject to the equality constraints

$$s_r = \boldsymbol{\psi}^T\varphi(\boldsymbol{G}_r) + b + e_r \tag{24}$$

where $\boldsymbol{\psi}$ is the weight vector, $\boldsymbol{G}_r = (\tau_r, d_r, t_r, a_r)$, $\varphi(\boldsymbol{G}_r)$ is the mapping function, b is the model parameter, e_r is the error vector, and γ is balancing parameters between equation size and training error.

Combining Equations (23) and (24), the Lagrangian is defined as

$$\mathrm{L}(\boldsymbol{\psi}, \boldsymbol{b}, \boldsymbol{e}, \boldsymbol{\sigma}) = \zeta(\boldsymbol{\psi}, \boldsymbol{b}, \boldsymbol{e}) - \sum_{r=1}^{R}\sigma_r\left\{[\boldsymbol{\psi}^T\varphi(\boldsymbol{G}_r) + \boldsymbol{b}] + e_r - 1\right\} \tag{25}$$

Equation (25) satisfies the following:

$$\frac{\partial L}{\partial \boldsymbol{\psi}} = \boldsymbol{\psi} - \sum_{r=1}^{R}\sigma_r s_r \varphi(\boldsymbol{G}_r) = 0 \tag{26}$$

$$\frac{\partial L}{\partial \boldsymbol{b}} = \sum_{r=1}^{R}\sigma_r s_r = 0 \tag{27}$$

$$\frac{\partial L}{\partial \boldsymbol{e}} = \gamma e_r - \sigma_r = 0 \tag{28}$$

$$\frac{\partial \boldsymbol{L}}{\partial \boldsymbol{\sigma}} = s_r[\boldsymbol{\psi}^T\varphi(\boldsymbol{G}_r) + \boldsymbol{b}] + e_r - 1 \tag{29}$$

The matrix form of Equations (26)–(29) can be expressed as:

$$\begin{bmatrix} 1 & 0 & 0 & -\boldsymbol{Z}^T \\ 0 & 0 & 0 & -\boldsymbol{s}^T \\ 0 & 0 & \boldsymbol{\gamma}^{\mathrm{I}} & -I \\ \boldsymbol{Z} & \boldsymbol{s} & I & 0 \end{bmatrix} \begin{bmatrix} \boldsymbol{\psi} \\ \boldsymbol{b} \\ \boldsymbol{e} \\ \boldsymbol{\sigma} \end{bmatrix} = \begin{bmatrix} 0 \\ 0 \\ 0 \\ \vec{1} \end{bmatrix} \tag{30}$$

where $\boldsymbol{Z} = [\varphi(\boldsymbol{G}_1)s_1, \varphi(\boldsymbol{G}_2)s_2, \cdots, \varphi(\boldsymbol{G}_r)s_r]$, $\boldsymbol{s} = [s_1, s_2, \cdots, s_r]$, $\boldsymbol{e} = [e_1, e_2, \cdots, e_r]$, and $\boldsymbol{\sigma} = [\sigma_1, \sigma_2, \cdots, \sigma_r]$, σ is the Lagrangian factor.

The kernel function matrix is defined as $\boldsymbol{K} = \boldsymbol{Z}\boldsymbol{Z}^T$. When the radial basis function (RBF) is selected as the kernel function, the mapping function is constructed as

$$K(\boldsymbol{G}, \boldsymbol{G}_r) = \exp\left(-\|\boldsymbol{G} - \boldsymbol{G}_r\|^2/\rho^2\right) \tag{31}$$

and Equation (31) is also given by

$$\begin{bmatrix} 0 & -\boldsymbol{s}^T \\ \boldsymbol{s} & \boldsymbol{K} + \gamma^{-1}I \end{bmatrix} \begin{bmatrix} \boldsymbol{b} \\ \boldsymbol{\sigma} \end{bmatrix} = \begin{bmatrix} 0 \\ \vec{1} \end{bmatrix} \tag{32}$$

Figures 2 and 3 show the flowcharts of the SSF forecasting methods based on the LSSVM considering the observation time parameter (represented as LSSVM-1) and the LSSVM considering multiple parameters (represented as LSSVM-2). For the LSSVM-1 method, the input layer of the training set is the matrix $[\tau_r, d_{r,1}, d_{r,2}, \cdots, d_{r,k}], r = 1, 2, \cdots, R, k = 1, 2, \cdots, K$. The output layer of the training set is $[s_{r,1}, s_{r,2}, \cdots, s_{r,k}], r = 1, 2, \cdots, R, k = 1, 2, \cdots, K$. The input layer of the forecasting set is $\left[\tau_f, d_{f,1}, d_{f,2}, \cdots, d_{f,k}\right]$. The output layer of the forecasting set is the estimated SSF at full ocean depth. For the LSSVM-2 method, the input layer of the training set is the matrix $\left[\tau_f, d_{r,k}, t_{r,k}, a_{r,k}\right]$ and the output layer of the training set is $[s_{r,1}, s_{r,2}, \cdots, s_{r,k}]$. The input layer of the forecasting set is $\left[\tau_f, d_{f,k}, t_{f,k}, a_{f,k}\right]$ and the output layer of the forecasting set is $s_{f,k}$. After that, the SSF at full ocean depth is estimated by repeating K times.

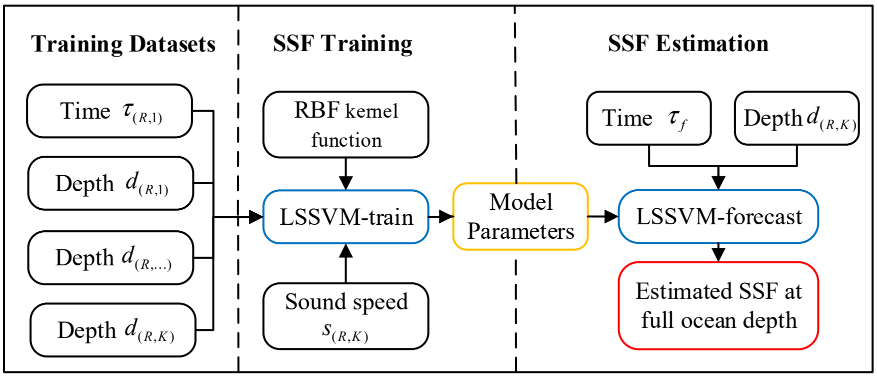

Figure 2. Flowchart for SSF forecasting using LSSVM-1.

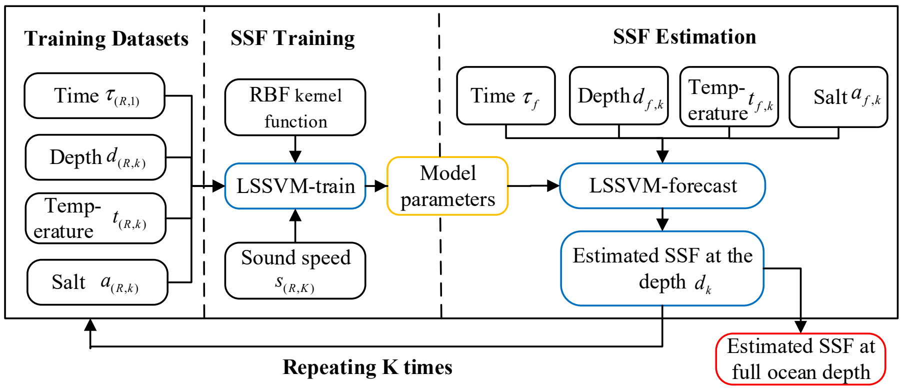

Figure 3. Flowchart for SSF forecasting using LSSVM-2.

4. Results

4.1. Measured Data

4.1.1. Matching Extension of SSPs, TPs, and SPs

The SSP, TP, and SP data for this experiment were collected by CTD and XCTD, including six sets of CTD data and nine sets of XCTD data. Figure 4 shows the numbers and observation times of the measured sound speed profile. As shown in Figure 4, these data were collected approximately one to two hours apart across the entire day. The observation times were 04:20, 07:00, 08:30, 10:30, 11:40, 13:00, 14:45, 17:20, 19:00, 20:00, 20:20, 20:30, 21:00, 23:00, and 23:35 on 28 March 2023.

Due to the influence of seawater movement during the data collection process, the gradient of the profile data does not increase linearly, and gross errors need to be eliminated. Figure 5 shows the preprocessed SSP, TP, and SP data. The data collected by CTD is lowered in the form of steel cables using a shipborne crane, with a measurement depth larger than 3000 m; and the data collected by XCTD is lowered using a projection gun firing method, with a measurement depth smaller than 2200 m. Therefore, the depth of the profile data of Figure 5 is unequal, which leads to the inability to construct the forecasting model of SSF based on the datasets of Figure 5.

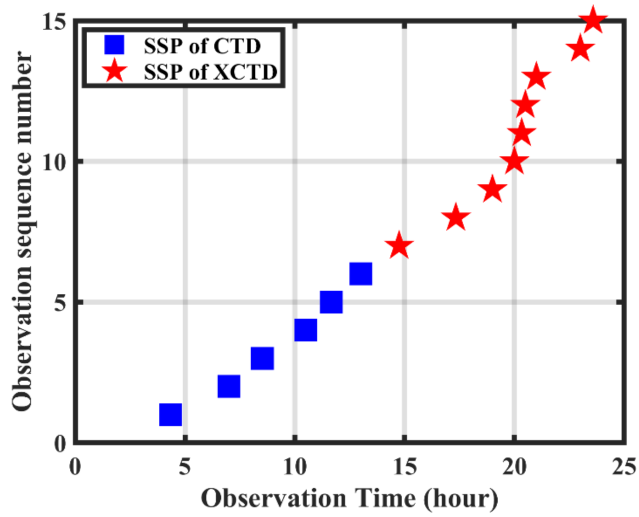

Figure 4. The number and observation time of CTD/XCTD data.

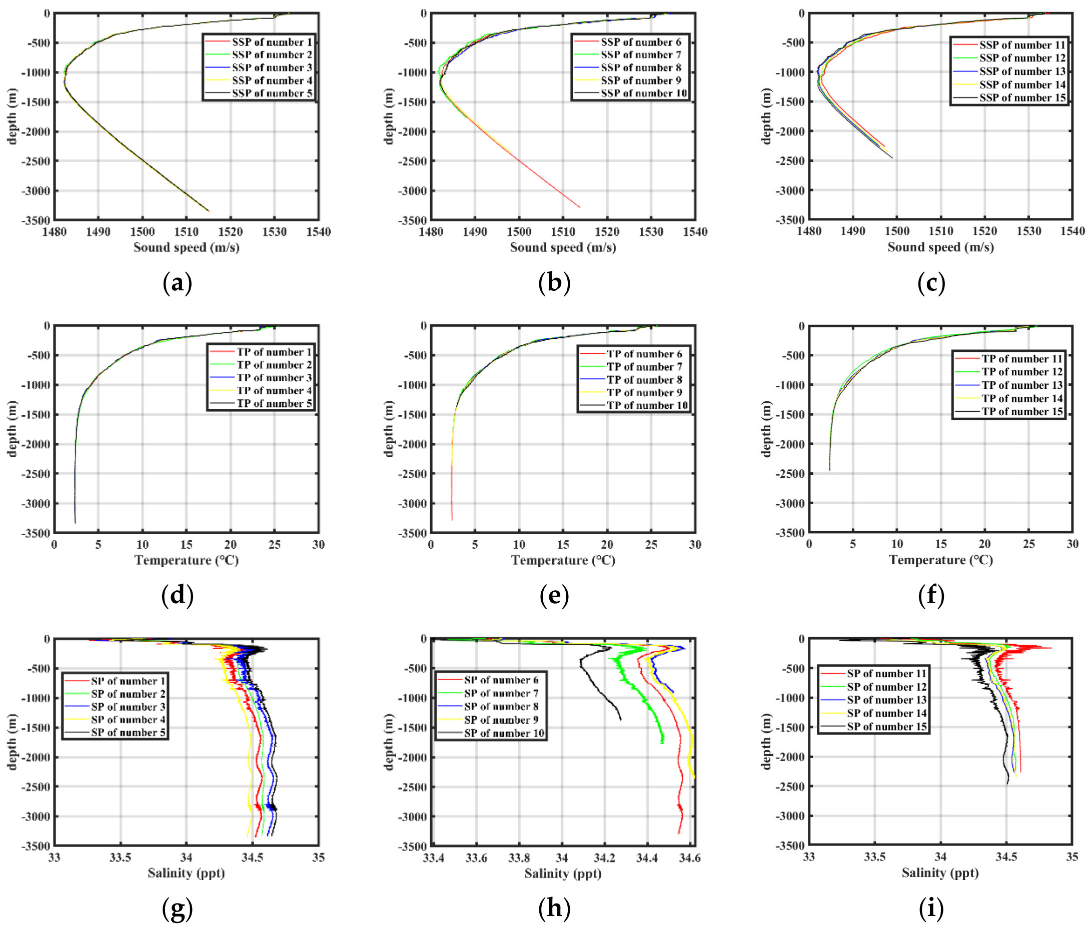

Figure 5. The distribution of the non-extended SSP, TP, and SP data. (**a**) The SSP of numbers 1–5; (**b**) the SSP of numbers 6–10; (**c**) the SSP of numbers 11–15; (**d**) the TP of numbers 1–5; (**e**) the TP of numbers 6–10; (**f**) the TP of numbers 11–15; (**g**) the SP of numbers 1–5; (**h**) the SP of numbers 6–10; (**i**) the SP of numbers 11–15.

Ensuring consistency in the format of data samples is a prerequisite for SSF forecasting. Therefore, the linear interpolation is firstly used to transform the profile data into 1 m intervals. Then, the minimum depth of 3349 m in CTD data is used as a reference sample to extend the XCTD data through linear interpolation and the matching extension method based on EOF. Figure 6 gives the extended SSP, TP, and SP data of equal intervals and the same depth. From the TP and SP data of Figure 6, the TP data varies between 2 °C and 25 °C and the SP data varies between 33 ppt and 35 ppt. These also indicate that the temperature and salinity both have an impact on the sound speed, and the temperature has a more significant impact on the sound speed than the salinity [31]. At the same time, the extended profiles are gained based on the matching extension method and the EOF. The change trend of the extended profile is same as the change trend of the reference profile, which also supports the reference profile data for the construction of the SSF forecasting model at full ocean depth.

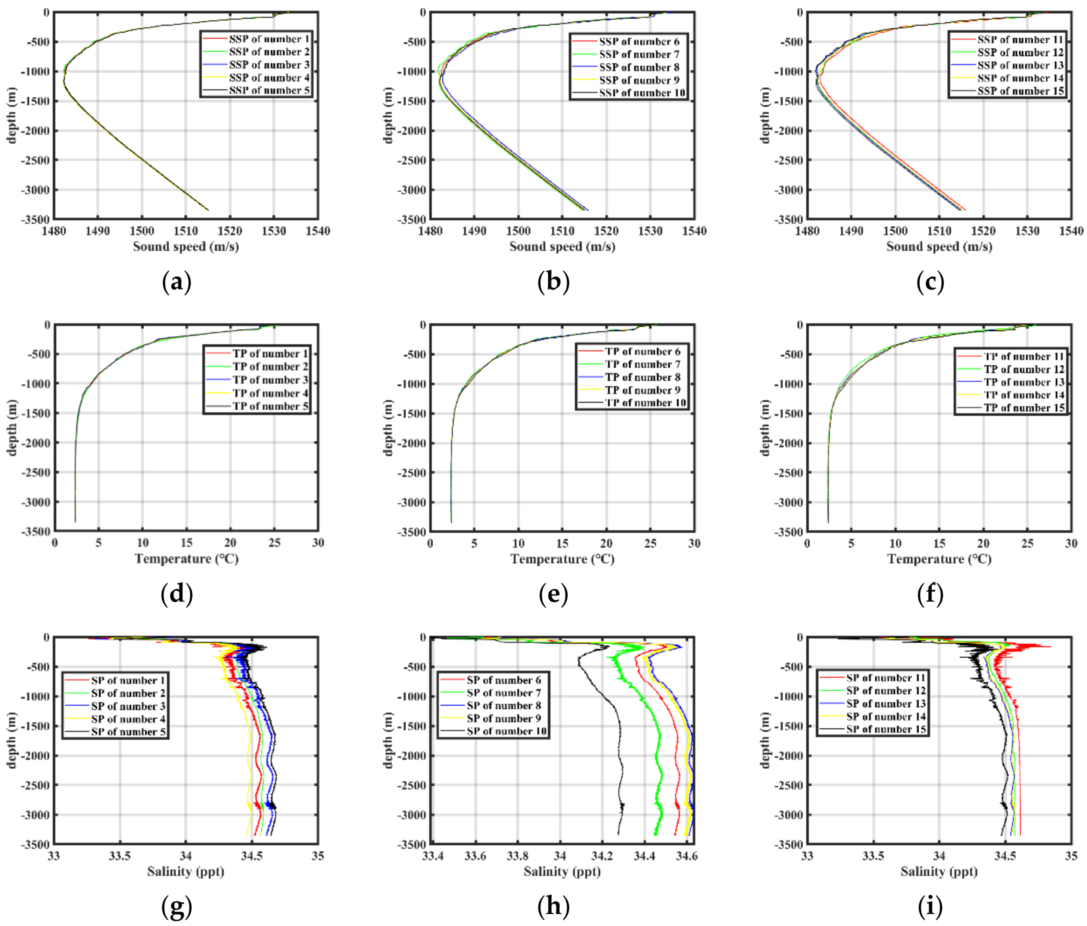

Figure 6. The distribution of the extended SSP, TP, and SP data. (**a**) The SSP of numbers 1–5; (**b**) the SSP of numbers 6–10; (**c**) the SSP of numbers 11–15; (**d**) the TP of numbers 1–5; (**e**) the TP of numbers 6–10; (**f**) the TP of numbers 11–15; (**g**) the SP of numbers 1–5; (**h**) the SP of numbers 6–10; (**i**) the SP of numbers 11–15.

4.1.2. Evaluation of the Inversion Accuracy of SSF

The polynomial fitting (PF) method, the BPNN method, the LSSVM considering the observation time parameter (represented as LSSVM-1), and the LSSVM considering multiple parameters (represented as LSSVM-2) are used to predict the SSPs of number 7 to number 15. We use previous datasets as reference SSPs to predict the SSP at later times. Figure 7 presents the variation of the sound speed field forecasting datasets for number 7 to number 15. The figure shows the observation time and the quantity of the training dataset for sound speed field forecasting. Figures 8–10 present the forecasting SSP, the test SSP, and the difference between the forecasting SSP and the test SSP of different algorithms in the representative SSPs of numbers 7, 10, and 13. From Figure 8, the forecasting accuracy of PF is better than that of LSSVM-1 and LSSVM-2. This is due to the strong consistency of the changing trend in temperature and salinity between the forecasting SSP and the reference SSP of Figure 7a. From Figure 6g,h, the salinity variation between the forecasting SSP of number 7 and the reference SSPs of numbers 1–6 is approximately 34.5 ppt, which makes the forecasting accuracy of PF better. The BPNN algorithm has the worst accuracy compared with the other methods. The reason is that the accuracy of BPNN is significantly worse than that of the LSSVM algorithm in small sample learning. For the SSPs of number 10 and number 13, the temperatures and salinity of the forecasting SSP and the reference SSP—shown in Figure 7d,g—vary greatly, which leads to the poor performance of the PF algorithm compared to the BPNN and LSSVM-1/2 algorithms in Figures 9 and 10. Furthermore, the LSSVM algorithm has the obvious advantage in small sample learning, and the LSSVM-2 algorithm can fully use the measured environmental parameters to construct the real SSF. Therefore, its construction accuracy is significantly improved compared with the PF, BPNN, and LSSVM-1 algorithms from Figures 9 and 10.

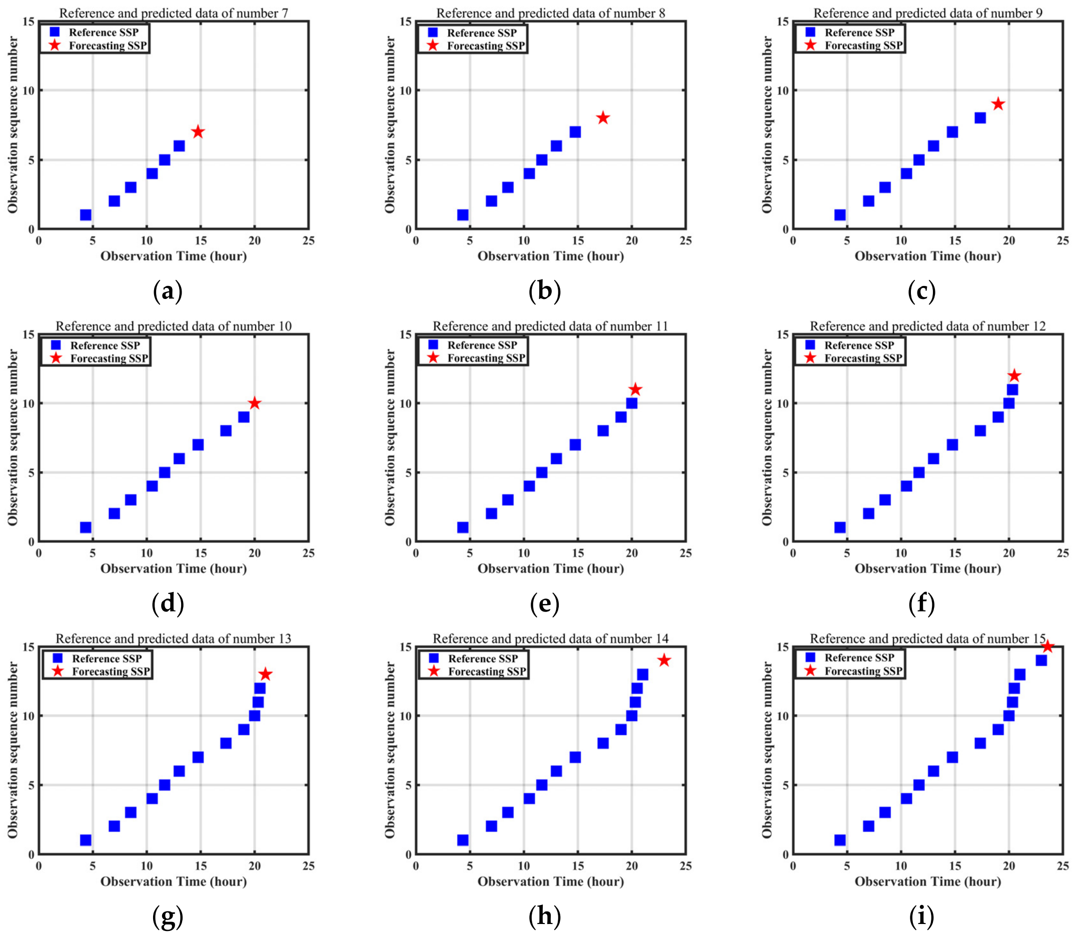

Figure 7. The variation chart of sound speed field forecasting datasets. (**a**) Number 7; (**b**) number 8; (**c**) number 9; (**d**) number 10; (**e**) number 11; (**f**) number 12; (**g**) number 13; (**h**) number 14; (**i**) number 15.

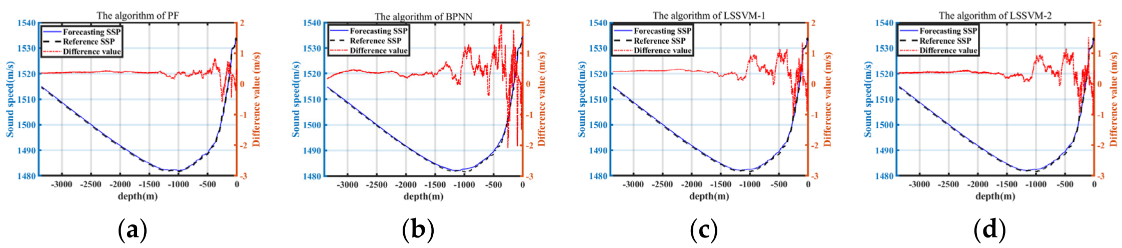

Figure 8. The comparison of the SSPs of number 7 predicted with different algorithms. (**a**) PF; (**b**) BPNN; (**c**) LSSVM-1; (**d**) LSSVM-2.

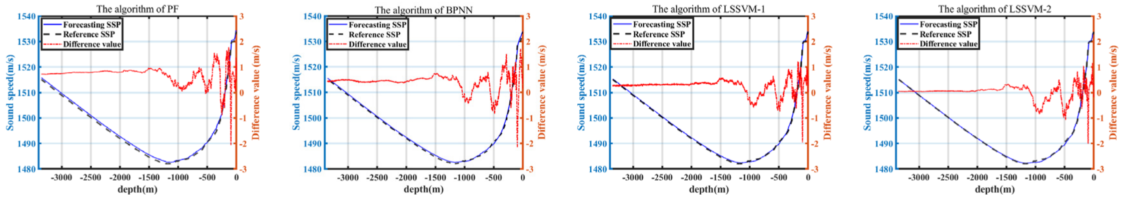

(**a**) (**b**) (**c**) (**d**)

Figure 9. The comparison of the SSPs of number 10 predicted with different algorithms. (**a**) PF; (**b**) BPNN; (**c**) LSSVM-1; (**d**) LSSVM-2.

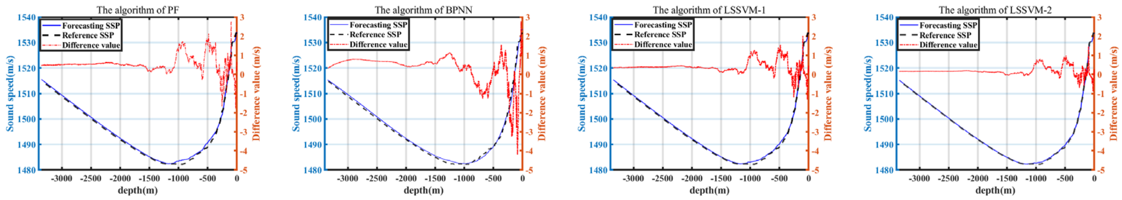

(**a**) (**b**) (**c**) (**d**)

Figure 10. The comparison of the SSPs of number 13 predicted with different algorithms. (**a**) PF; (**b**) BPNN; (**c**) LSSVM-1; (**d**) LSSVM-2.

In order to evaluate the accuracy of different depth layers for the nine selected forecasting samples, the results of the root mean square (RMS) for the full ocean depth, the surface layer (0–550 m), the thermocline (551–1500 m), and the deep-sea isotherm (>1500 m) are counted and shown in Figure 11. The root mean square (RMS) is expressed as

$$RMS = \sqrt{\frac{\sum_{j=\vartheta}^{\zeta}\left[s_f(d_j) - s_r(d_j)\right]^2}{(\zeta - \vartheta + 1)}} \tag{33}$$

where ζ and ϑ are the initial and maximum depth of the full ocean depth, the surface layer, the thermocline, and the deep-sea isotherm. $s_f(d_j)$ and $s_r(d_j)$ are the forecasting sound speed and the real value of the forecasting SSP.

From Figure 11, the accuracy of both LSSVM-1 and LSSVM-2 has significant improvement in the full ocean depth compared with the PF algorithm. When there are significant changes in the marine environment, the BPNN algorithm is better than the PF algorithm, and its forecasting accuracy is maintained at about 1 m/s. In the surface layer and the thermocline, the accuracy of the PF and the BPNN algorithms are significantly poor due to the drastic changes of the temperature and the salinity, as well as insufficient training samples, while LSSVM-1/-2 still keep the accuracy of about 0.6 m/s and 0.5 m/s in the surface layer and the thermocline. In the deep-sea isotherm, the SSF with hourly resolution is affected by the variation of the temperature and the salinity, which leads to the lower accuracy of the PF algorithm. The forecasting accuracy of BPNN and LSSVM-2 for number 11 decreases in Figure 11; the reason is that the salinity level of number 11 fluctuates greatly and it is significantly different from the salinity change in the training sample (number 1–number 10) from Figure 6g–i. Therefore, when the salinity changes greatly between the forecast sample and the training sample, it affects the accuracy of BPNN and LSSVM based on multiple parameters. Compared with PF and LSSVM-1, the accuracy of LSSVM-2 is reduced, but within an acceptable range. Except for the forecast sample of number 11, LSSVM-2 can consider the temperature and salinity parameter to construct the forecasting model of SSF, which significantly improves the forecasting accuracy of SSFs.

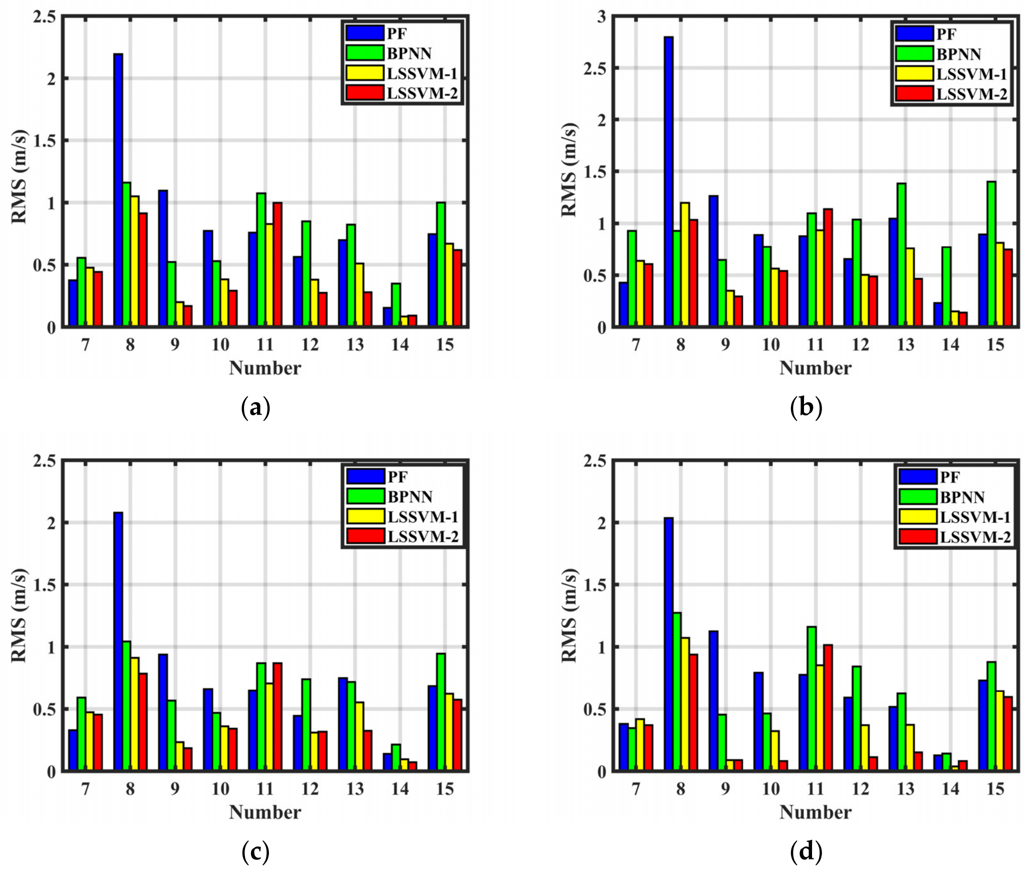

Figure 11. The RMSs of the forecasting SSP for the different algorithms and the different depths. (**a**) Full ocean depth; (**b**) surface layer; (**c**) thermocline; (**d**) deep-sea isotherm.

After that, the maximum, minimum, and mean of the RMSs for the different algorithms in different seawater stratifications, as well as the accuracy improvement percentage of LSSVM-1 and LSSVM-2 relative to the PF and BPNN methods in the mean of the RMS, are statistically analyzed in Table 1. Regarding the maximum RMS of four of the methods, that of PF is largest, with a value greater than 2 m/s in different seawater layers. The maximum RMS for the other three algorithms is significantly reduced, and that of LSSVM-2 is the smallest and maintains approximately 1 m/s in different seawater layers. Compared with the other three algorithms, the minimum RMS for LSSVM-2 is the smallest, with a value less than 0.1 m/s in different seawater layers. The above results indicate that the PF algorithm only considering the observation time has poor forecasting accuracy of SSFs. However, the BPNN and LSSVM algorithms with good nonlinear function-fitting ability can significantly improve forecasting accuracy. For the full ocean depth, the mean of RMS for LSSVM-1 is 0.51 m/s, with an improvement of 37.7% and 33.2% compared to the 0.82 m/s of PF and the 0.76 m/s of BPNN. Using the improved strategy of the inversion model based on multiple parameters, the mean of RMS for LSSVM-2 is 0.452 m/s, with a notable improvement of 44.6% and 40.6% compared to the 0.82 m/s of PF and the 0.76 m/s of BPNN. In the surface layer, the mean of RMS for LSSVM-1 is 0.66 m/s, with an improvement of 34.9% and 34.1% compared to the 1.01 m/s of PF and the 0.10 m/s of BPNN. Using the improved strategy of the inversion model based on multiple parameters, the mean of RMS for LSSVM-2 is 0.61 m/s, with an improvement of 39.8% and 39.1% compared to the 1.01 m/s of PF and the 1.00 m/s of BPNN. Within the thermocline, the mean of RMS for LSSVM-1 is 0.47 m/s, with an improvement of 36.0% and 30.6% compared to the 0.74 m/s of PF and the 0.68 m/s of BPNN. Using the improved strategy of the inversion model based on multiple parameters, the mean of RMS for LSSVM-2 is 0.44 m/s, resulting in an improvement of 41.2% and 36.3% compared to the 0.74 m/s of PF and the 0.68 m/s of BPNN. In the deep-sea isotherm, the mean of RMS for

LSSVM-1 is 0.47 m/s, with an improvement of 40.8% and 32.3% compared to the 0.77 m/s of PF and the 0.69 m/s of BPNN. Using the improved strategy of the inversion model based on multiple parameters, the mean of RMS for LSSVM-2 is 0.38 m/s, with an improvement of 51.4% and 44.4% compared to the 0.79 m/s of PF and the 0.69 m/s of BPNN. According to the above results, the RMS for the LSSVM algorithm is less than that of the PF and BPNN algorithm; the reason is that the LSSVM algorithm is more suitable for the training of small samples and can achieve more complex nonlinear function fitting in high dimensional space. Compared with LSSVM-1, LSSVM-2 has higher forecasting precision due to its consideration of multiple parameters.

Table 1. The statistical results of the different algorithms.

Method	Statistics	Full Ocean Depth (m/s)	Surface Layer (m/s)	Thermocline (m/s)	Isothermal Layer (m/s)
PF	Maximum RMS	2.19	2.80	2.07	2.04
	Minimum RMS	0.15	0.23	0.14	0.13
	Mean of RMS	0.82	1.01	0.74	0.79
BPNN	Maximum RMS	1.16	1.40	1.04	1.27
	Minimum RMS	0.35	0.64	0.22	0.14
	Mean of RMS	0.76	1.00	0.68	0.69
LSSVM-1	Maximum RMS	1.05	1.20	0.91	1.07
	Minimum RMS	0.09	0.15	0.10	0.04
	Mean of RMS	0.51	0.66	0.47	0.47
LSSVM-2	Maximum RMS	1.00	1.14	0.87	1.01
	Minimum RMS	0.09	0.14	0.07	0.08
	Mean of RMS	0.45	0.61	0.44	0.38
Improvement percentage of LSSVM-1 relative to PF (%)	Mean of RMS	37.7	34.9	36.0	40.8
Improvement percentage of LSSVM-2 relative to PF (%)	Mean of RMS	44.6	39.8	41.2	51.4
Improvement percentage of LSSVM-1 relative to BPNN (%)	Mean of RMS	33.2	34.1	30.6	32.3
Improvement percentage of LSSVM-2 relative to BPNN (%)	Mean of RMS	40.6	39.1	36.3	44.4

4.2. Public Data Sources

In order to further verify the accuracy of the LSSVM based on multiple parameters proposed in this paper, we chose the marine environmental data of January 2011, released by the National Oceanic and Atmospheric Administration of the United States, as validation datasets. The temporal resolution of the data is hours and the data includes 12 vertical levels from 1.5 m to 750 m. Each data point includes the information of temperature, salinity, sound speed, and depth. The above environmental data of one week is selected as the validation dataset for the SSP forecasting. Similarly, the datasets of past times are used as reference SSPs to predict the SSP in the future. Figure 12 shows the observation times of the reference SSPs and forecasting SSPs for 137 groups within one week. The observation time is calculated by hours within one week.

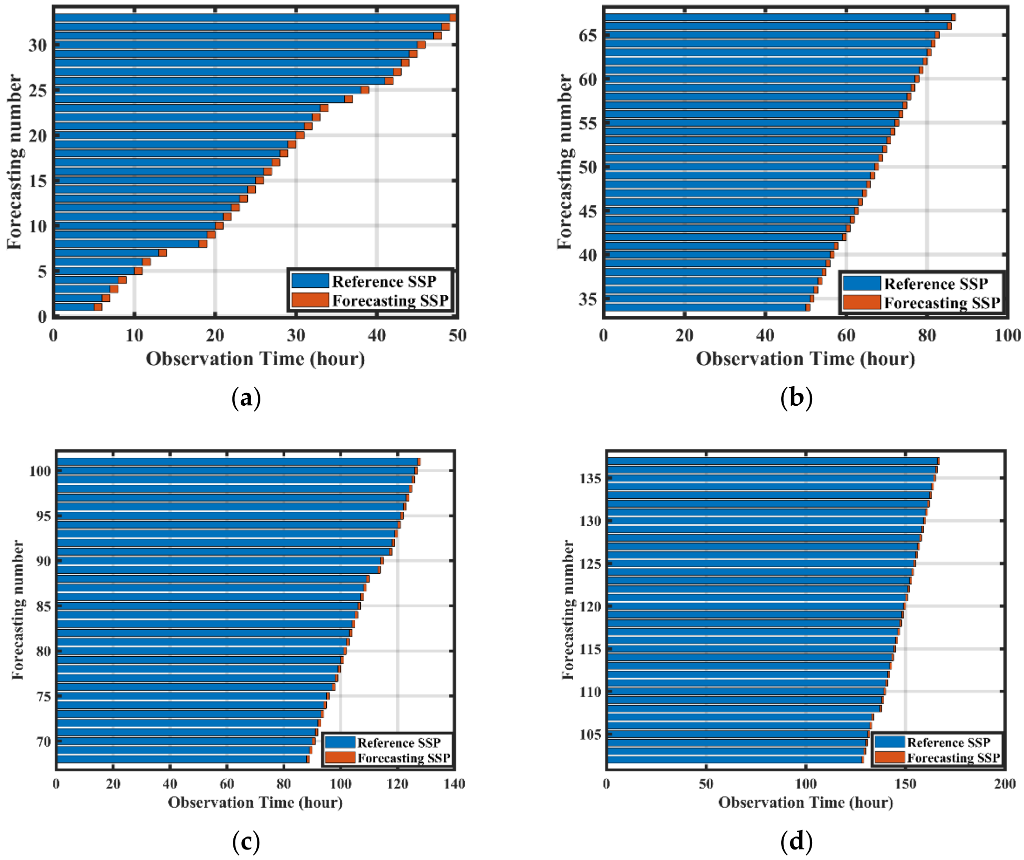

Figure 12. The variation chart of sound speed field forecasting datasets. (**a**) Numbers 1–33; (**b**) numbers 34–67; (**c**) numbers 68–101; (**d**) numbers 102–137.

The PF, BPNN, LSSVM-1, and LSSVM-2 methods are used to predict the SSPs of 137 groups in Figure 12. Figure 13 shows the nearest reference SSPs and forecasting SSPs of the representative SSPs for the numbers 28, 62, 96, and 130. The variation trend of the nearest reference SSPs and forecasting SSPs of the numbers 28 and 62 is similar, while the SSPs of the numbers 96 and 130 have a significant difference in variation trends at a depth of 150 m. Figures 14–17 present the forecasting SSPs, the test SSPs, and the differences between the forecasting SSPs and the test SSPs of the different algorithms in the representative SSPs of the numbers 28, 62, 96, and 130. From Figure 14, the forecasting accuracy of LSSVM-1 is better than that of PF and BPNN, and the accuracy of LSSVM-2 has more significant improvement compared with PF, BPNN, and LSSVM-1. Especially at a depth of 150 m, the difference between the forecasting SSP and the test SSP of LSSVM-2 is smaller. From Figure 15, the forecasting accuracy of BPNN is better than that of PF and LSSVM-1, and the accuracy of LSSVM-2 has the best forecasting results of SSFs. The above results indicate that as the number of samples increases, the accuracy of the forecasting models based on BPNN and LSSVM considering multiple parameters is better. However, the accuracy of LSSVM based on multiple parameters is better compared with that of BPNN. From Figures 16 and 17, the forecasting results of PF are poor, while the LSSVM-1 and LSSVM-2 algorithms have better performances. The difference between the forecasting SSP and the test SSP of the BPNN algorithm is significantly large at a depth of 150 m; the reason for the above results is that the sound speed of the reference samples near the forecast samples changes significantly from Figure 13. However, the forecasting accuracy of the LSSVM considering multiple parameters still has significant improvement.

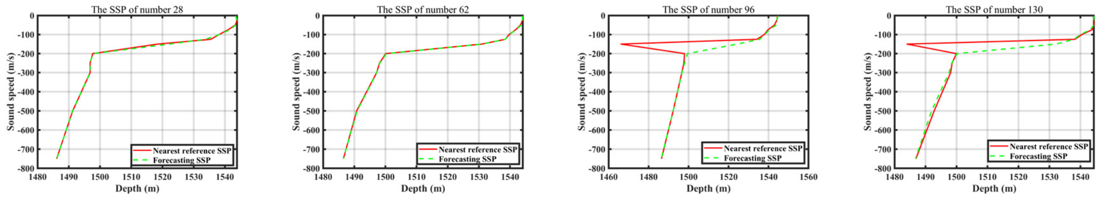

(**a**) (**b**) (**c**) (**d**)

Figure 13. The nearest reference SSPs and forecasting SSPs of the different forecasting times. (**a**) Number 28; (**b**) number 62; (**c**) number 96; (**d**) number 130.

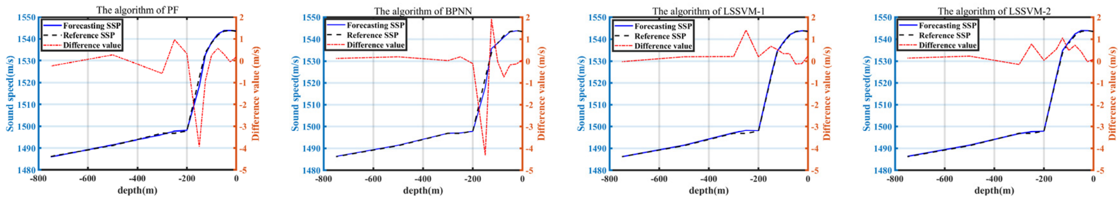

(**a**) (**b**) (**c**) (**d**)

Figure 14. The comparison of the SSPs of number 28 for the different algorithms. (**a**) PF; (**b**) BPNN; (**c**) LSSVM-1; (**d**) LSSVM-2.

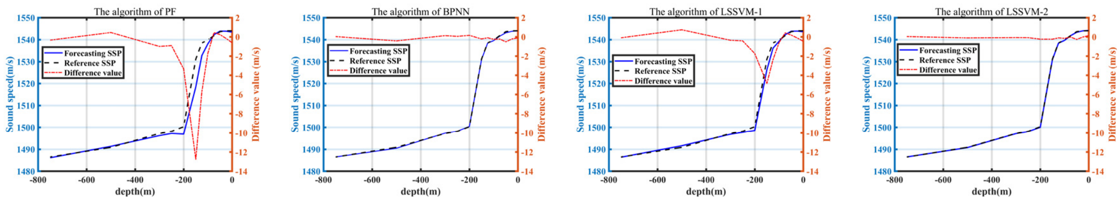

(**a**) (**b**) (**c**) (**d**)

Figure 15. The comparison of the SSPs of number 62 for the different algorithms. (**a**) PF; (**b**) BPNN; (**c**) LSSVM-1; (**d**) LSSVM-2.

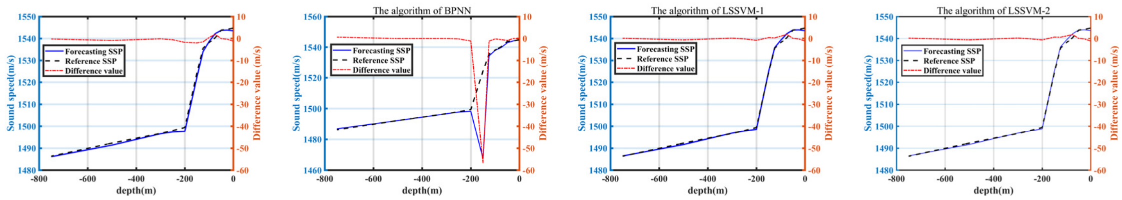

(**a**) (**b**) (**c**) (**d**)

Figure 16. The comparison of the SSPs of number 96 for the different algorithms. (**a**) PF; (**b**) BPNN; (**c**) LSSVM-1; (**d**) LSSVM-2.

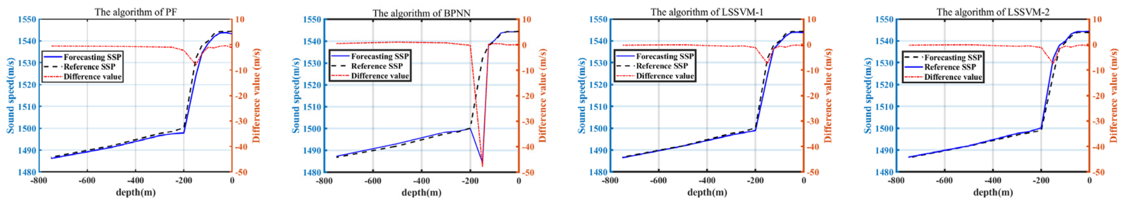

(**a**) (**b**) (**c**) (**d**)

Figure 17. The comparison of the SSPs of number 130 for the different algorithms. (**a**) PF; (**b**) BPNN; (**c**) LSSVM-1; (**d**) LSSVM-2.

In order to evaluate the accuracy in detail, the difference between the reference and forecasting SSPs and the RMSs of the forecasting SSPs for the different algorithms are counted and shown in Figure 18. Compared with the PF, the BPNN and the LSSVM-1 algorithms, the difference of LSSVM-2 fluctuates around zero and the undulation scope is smaller. The RMS of LSSVM-2 has a significant decrease in accuracy compared to the other three methods. Table 2 presents the mean and maximum values of the differences between the different depths and algorithms. For the depth of 50 m, the mean and maximum values of LSSVM-2 can improve from (−0.31, 1.20) m/s, (−0.16, 1.00) m/s, and (−0.24, 1.31) m/s to (−0.04, 0.73) m/s compared with PF, BPNN, and LSSVM-1. For the depth of 150 m, the mean and maximum values of LSSVM-2 can improve from (−5.45, 15.43) m/s, (−0.46, 59.66) m/s, and (−1.90, 9.90) m/s to (−0.29, 7.57) m/s compared with PF, BPNN, and LSSVM-1. For the depth of 750 m, the mean and maximum values of LSSVM-2 can improve from (−0.44, 1.76) m/s, (−0.13, 1.41) m/s, and (−0.22, 1.42) m/s to (−0.05, 1.40) m/s compared with PF, BPNN, and LSSVM-1. After that, the means of the RMSs for different algorithms, as well as the accuracy improvement percentage of LSSVM-1/2 relative to PF and BPNN, are statistically analyzed and shown in Table 3. The mean of the RMS for LSSVM-1 is 1.35 m/s compared to the 2.63 m/s of PF and the 1.77 m/s of BPNN, with an improvement of 48.8% and 23.7%. Using the improved strategy of the inversion model based on multiple parameters, the RMS of LSSVM-2 is 0.64 m/s compared to the 2.63 m/s of PF and the 1.77 m/s of BPNN, with an improvement of 75.8% and 63.9%. Therefore, compared with PF, the mean of RMS for BPNN in full ocean depth is smaller. The LSSVM-2 algorithm not only considers multiple parameters, but is not affected by the changing of sound speed in adjacent training samples, which significantly improves its forecasting accuracy of SSFs.

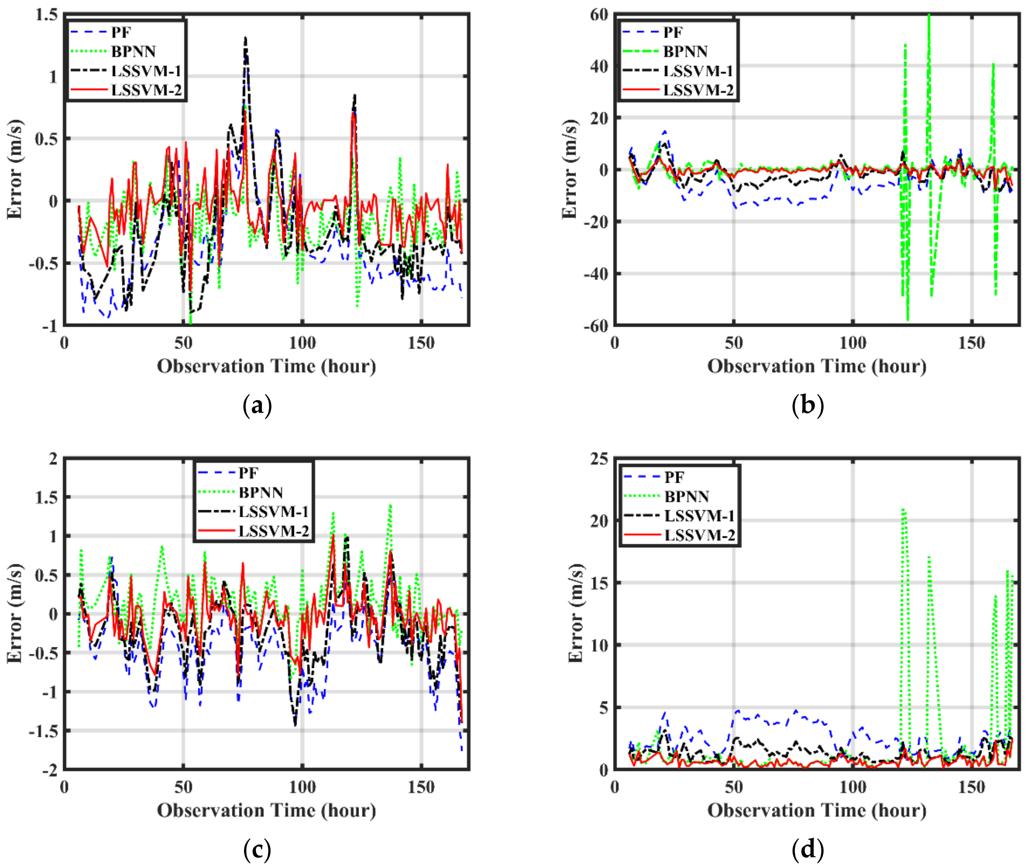

Figure 18. The difference between the reference and forecasting SSPs and the RMSs of the forecasting SSPs for the different algorithms. (**a**) Difference of depth 50 m; (**b**) difference of depth 150 m; (**c**) difference of depth 750 m; (**d**) RMS of full ocean depth.

Table 2. The mean and maximum values of the differences between the different depths and methods.

Depth	Statistics	PF	BPNN	LSSVM-1	LSSVM-2
Difference of depth 50 m	Mean Max	−0.31 1.20	−0.16 0.99	−0.24 1.31	−0.04 0.73
Difference of depth 150 m	Mean Max	−5.45 15.43	−0.46 59.66	−1.90 9.90	−0.29 7.57
Difference of depth 750 m	Mean Max	−0.44 1.76	0.13 1.41	−0.22 1.42	−0.05 1.40

Table 3. The mean RMS of the different algorithms and the accuracy improvement of LSSVM-1 and LSSVM-2.

Method	PF	BPNN	LSSVM-1	LSSVM-2
Mean RMS of full ocean depth (m/s)	2.63	1.77	1.35	0.64
Improvement percentage relative to PF (%)	-	-	48.8	75.8
Improvement percentage relative to BPNN (%)	-	-	23.7	63.9

5. Conclusions

The irregular changes of ocean sound speed can cause significant acoustic observation errors in underwater acoustic observations. To construct a high-precision SSF with hourly resolution, this paper proposes an inversion method considering multiple parameters, based on the LSSVM algorithm and a matching extension technique. The following conclusions are drawn from experimental analysis and comparison.

(1) The matching extension method uses EOF decomposition to perform principal component analysis for profile information, thereby achieving the profile extension in the full ocean depth. The extended profile exhibits a similar trend to the reference profile, which provides crucial reference data for constructing the SSF forecasting model for the entire ocean depth.

(2) For the measured data, when the forecasting SSPs and the reference SSPs have significant consistency, the polynomial fitting algorithm has higher accuracy. However, when the forecasting SSPs and the reference SSPs have significant differences, the accuracy of the polynomial fitting algorithm is greatly reduced. When there are significant changes in the marine environment, the BPNN algorithm is better than the PF algorithm, and its forecasting accuracy is affected by the number of training samples. The RMS of the full ocean depth for the proposed LSSVM algorithm based on the observation time is 0.51 m/s, with an improvement of 37.7% and 33.2% compared to the 0.82 m/s of PF and the 0.76 m/s of BPNN. By using an improved strategy of the multi-parameter model, the improved LSSVM can further improve the accuracy of sound speed field prediction. The mean of the RMS of the full ocean depth for the improved LSSVM algorithm based on the multi-parameter model is 0.45 m/s, with an improvement of 44.6% and 40.6% compared to the 0.82 m/s of PF and the 0.76 m/s of BPNN. The above results indicate that the LSSVM considering the multi-parameter model has the highest forecasting accuracy. The reason is that the algorithm is more suitable for the training of small samples and considers multiple parameters in order to better express the sound speed.

(3) For the public data, using the ability of linear least squares in high dimensional space, the LSSVM algorithm can improve the forecasting accuracy of sound speed fields by combining measured temperature, salinity, and pressure data. The mean of the RMS for LSSVM-1 is 1.35 m/s, with an improvement of 48.8% and 23.7% compared to the 2.63 m/s of PF and the 1.77 m/s of BPNN. The mean of the RMS for LSSVM-2 is

0.636 m/s, with an improvement of 75.8% and 63.9% compared to the 2.63 m/s of PF and the 1.77 m/s of BPNN. Consequently, this LSSVM considering multiple parameters can construct a high-precision sound speed field with hourly resolution, which offers sound speed corrections for underwater acoustic positioning and navigation.

Author Contributions: J.W.: conceptualization, methodology, formal analysis, investigation, software, original draft writing. T.X.: conceptualization, methodology, project administration. W.H.: conceptualization, methodology. L.Z.: writing—review and editing. Y.L.: supervision, writing—review and editing. J.S.: writing—review and editing. L.L.: writing—review and editing. All authors have read and agreed to the published version of the manuscript.

Funding: This study is financially supported by the National Natural Science Foundation of China (42304011); the Shandong Provincial Natural Science Foundation (ZR2023QD163); the China Postdoctoral Science Foundation (2023M732041); the Shandong Provincial Natural Science Foundation (ZR2023QF128); and the Open Foundation of the State Key Laboratory of Geo-Information Engineering (SKLGIE2022-ZZZ-02).

Institutional Review Board Statement: Not applicable.

Informed Consent Statement: Not applicable.

Data Availability Statement: The measured data presented in this study are available from the corresponding author on request. The public data sources for this study can be found on the official website of the National Oceanic and Atmospheric Administration of the United States (https://www.pmel.noaa.gov/tao/drupal/disdel/).

Conflicts of Interest: The authors declare no conflicts of interest.

Abbreviations

The following abbreviations are used in this manuscript:

SSF	Sound Speed Field
LSSVM	Least Square Support Vector Machine
EOF	Empirical Orthogonal Function
SSPs	Sound Speed Profiles
TPs	Temperature Profiles
SPs	Salinity Profiles
RBF	Radial Basis Function
CTD	Conductivity–Temperature–Depth
XCTD	Expendable Conductivity–Temperature–Depth
RMS	Root Mean Square
PNTC	Positioning, navigation, timing, and communication
SSP	Sound speed profiler
SVD	Singular value decomposition
PSO	Particle swarm optimization
SA	Simulated annealing
GA	Genetic algorithm

References

1. Yang, Y. Concept of comprehensive PNT and related key technologies. *Acta Geod. Cartogr. Sin.* **2016**, *45*, 205–510.
2. Yang, Y. Resilient PNT Concept Frame. *Acta Geod. Cartogr. Sin.* **2018**, *47*, 893–898.
3. Yang, Y.; Yang, C.; Ren, X. PNT intelligent services. *Acta Geod. Cartogr. Sin.* **2021**, *50*, 1006–1012.
4. Xue, S.; Li, B.; Xiao, Z.; Sun, Y.; Li, J. Centimeter-level-precision seafloor geodetic positioning model with self-structured empiricasound speed profile. *Satell. Navig.* **2023**, *4*, 30. [CrossRef]
5. Huang, Y.; Guo, W.S. Spatial correlation of the acoustic vector field of the surface noise in three-dimensional ocean environments. *J. Acoust. Soc. Am.* **2014**, *135*, 2397. [CrossRef]
6. Worcester, P.F.; Munk, W.H. Ocean acoustic tomography: Fortieth anniversary, 1976–2016. *J. Acoust. Soc. Am.* **2016**, *140*, 2976. [CrossRef]
7. Zhang, L.; Ye, S.; Zhou, S.; Liu, F.; Han, Y. Review of Measurement Techniques for Temperature, Salinity and Depth Profile of Sea Water. *Mar. Sci. Bull.* **2017**, *36*, 481–489.

8. Munk, W.; Wunsch, C. Ocean acoustic tomography: A scheme for large scale monitoring. *Deep-Sea Res. (Oceanogr. Res. Pap.)* **1979**, *26*, 123–161. [CrossRef]
9. Michael, B.; Peter, G. Dictionary Learning of Sound Speed Profiles. *J. Acoust. Soc. Am.* **2017**, *141*, 1749–1758.
10. Tolstoy, A. Linearization of the matched-field processing approach to acoustic tomography. *J. Acoust. Soc. Am.* **1992**, *91*, 781–787. [CrossRef]
11. Zhang, Z.; Ma, Y.; Yang, K.; Yan, S. Inversion for sound speed profile in shallow water using matched-beam processing. *Acta Acust.* **2005**, *30*, 103–107. (In Chinese)
12. Tang, J.F.; Yang, S.E. Sound speed profile in ocean inverted by using travel time. *J. Harbin Eng. Univ.* **2006**, *27*, 734–756. (In Chinese)
13. Davis, R.E. Predictability of Sea Surface Temperature and Sea Level Pressure Anomalies over the North Pacific Ocean. *J. Phys. Ocean.* **1976**, *6*, 249–266. [CrossRef]
14. Bianco, M.J.; Gerstoft, P.; Traer, J.; Ozanich, E.; Roch, M.A.; Gannot, S.; Deledalle, C.A. Machine Learning in Acoustics: Theory and Applications. *J. Acoust. Soc. Am.* **2019**, *146*, 3590–3628. [CrossRef] [PubMed]
15. Tolstoy, A.; Diachok, O.; Frazer, L.N. Acoustic tomography via matched field processing. *J. Acoust. Soc. Am.* **1991**, *89*, 1119–1127. [CrossRef]
16. Zhang, W.X.; Gao, G.D.; Mu, G.Y. Research on modeling seawater salinity based on BP neural network. *Ocean Technol.* **2006**, *25*, 3.
17. Sun, W.; Bao, J.; Jin, S.; Xiao, F.; Cui, Y. Inversion of Sound Speed Profiles by Correcting the Terrain Distortion. *Geomat. Inf. Sci. Wuhan Univ.* **2016**, *41*, 349–355.
18. Michael, B.; Peter, G. Compressive Acoustic Sound Speed Profile Estimation. *J. Acoust. Soc. Am.* **2016**, *139*, EL90–EL94.
19. Choo, Y.; Seong, W. Compressive Sound Speed Profile Inversion Using Beamforming Results. *Remote Sens.* **2018**, *10*, 704. [CrossRef]
20. Wang, J.; Xu, T.; Nie, W.; Yu, X. The Construction of Sound Speed Field Based on Back Propagation Neural Network in the Global Ocean. *Mar. Geod.* **2020**, *43*, 1–14. [CrossRef]
21. Yann, S.; Sylvie, T.; Fouad, B. Inverting Tomographic Data with Neural Nets. In Proceedings of the 'Challenges of Our Changing Global Environment', OCEANS '95 MTS/IEEE, San Diego, CA, USA, 9–12 October 1995; pp. 1501–1504.
22. Ai, R.F.; Cheng, J.; Ouyang, J.; Yang, J. On-line retrieval methodology for sound speed profile of sea area. *J. Comput. Appl.* **2015**, *35*, 5.
23. Huang, W.; Li, D.S.; Jiang, P. Underwater Sound Speed Inversion by Joint Artificial Neural Network and Ray Theory. In Proceedings of the International Conference on Underwater Networks and Systems, Shenzhen, China, 3–5 December 2018; pp. 1–8.
24. Zhang, X.; Zhang, Y.G.; Zhang, J.X.; Dong, N. A new parameterization method for sound velocity profile structure. *J. Oceanogr.* **2011**, *33*, 54–60.
25. Luo, Z.H.; Lu, B.; Yang, Y. Application of Artificial Neural Network Technology in Sound Velocity Prediction for Marine Sediments. *Ocean Technol.* **2009**, *28*, 41–57.
26. Liu, B.S.; Lei, J.Y. *The Principles of Hydro-Acoustics*, 2nd ed.; Harbin Institute of Technology Press: Harbin, China, 2011.
27. Yu, X.K.; Xu, T.H.; Wang, J.T. Sound Velocity Profile Prediction Method Based on RBF Neural Network. In Proceedings of the China Satellite Navigation Conference (CSNC) 2020 Proceedings: Volume III, Chengdu, China, 22–25 November 2020; pp. 475–487.
28. Ji, C.Y.; Liu, C. Model experiment of intelligent control for deep water jack-up platforms based on BP neural network. *Ocean Eng.* **2013**, *31*, 19–27.
29. Cherkassky, V.; Ma, Y. Practical selection of SVM parameters and noise estimation for SVM regression. *Neural Netw.* **2004**, *17*, 113–126. [CrossRef] [PubMed]
30. Suykens, J. Least Squares Support Vector Machines. *Int. J. Circuit Theory Appl.* **2002**, *27*, 605–615. [CrossRef]
31. Tao, Z.D.; Wang, Y.Q.; Lu, Z.J. Study on the comparison and correction method of far-reaching sea sound velocity data. *Hydrogr. Surv. Charting* **2020**, *40*, 20–24.